Gain-scheduled linear-quadratic-regulator synthesis for the centre of gravity variations of Boeing 747-100 longitudinal modes

Elarbi, E. M., Laila, D. S. & Horri, N. M.

DOI 10.19101/IJATEE.2021.875709
ISSN 2394-5443
ESSN 2394-7454

Publisher: ACCENTS

International Journal of Advanced Technology and Engineering Exploration, Vol 9(92)
ISSN (Print): 2394-5443 ISSN (Online): 2394-7454
http://dx.doi.org/10.19101/IJATEE.2021.875709

Research Article

Gain-scheduled linear-quadratic-regulator synthesis for the centre of gravity variations of Boeing 747-100 longitudinal modes

Ezzeddin M. Elarbi[1*], Dina S. Laila[2] and Nadjim M. Horri[3]
The University of Tripoli, Aeronautical Engineering Department, Tripoli-Libya[1]
The Futures Institute, Coventry University Unit 10, Coventry CV1 2TL, the UK[2]
Aerospace engineering, Coventry University Priory Street, Coventry, the United Kingdom, CV1 5FB[3]

Received: 30-March-2022; Revised: 22-July-2022; Accepted: 25-July-2022

Abstract
For the variation in the centre of gravity (CG) of Boeing 747-100 (B747-100) longitudinal flight, the gain scheduling (GS) method is proposed to manage it over the flight envelope. The full-state feedback linear quadratic regulator (FSFLQR) has been synthesised with the GS, named (GS-FSFLQR), to obtain a realistic controller for Mach numbers (M) and altitudes (H) envelope. Such a practised control law demonstrates the CG mean aerodynamic chord (MAC) shifts correlated with M-H and actuator actions. The intermediate variable responses have been accomplished at (M, H) simulations of (0.2, 0), (0.5, 6096 m) and (0.9, 12190 m). Local controllers at M and H scheduled parameters are gained using the cubic spline method of 0.2 to 0.9 and sea level to 12190 m. Swift levelled convergences illustrated the B747-100 CG variations throughout most responses for a coupled elevator and throttle-controlled flight. These findings are validated for the flying quality requirements showing the competent merits of the GS-FSFLQR as opposed to without control flight. The maximum elevator capacity transmits the CG from the 17% MAC at (0.3, 6096 m) to 30% MAC at (0.7, 3048 m), whereas the maximum throttle occurs for the CG at 25% MAC at (0.5, 6096 m). Their minimum operations lead to 22% MAC at (0.6, sea level). The dominated CG location of the elevator is fore than 25% MAC whereas the aft and fore locations of the throttle float around that. 50% actuator effectiveness due to operable elevator and throttle adequately copes with the CG longitudinal stability.

Keywords
Boeing 747-100 flight envelope, Tracking longitudinal modes, Elevator and throttle coupling, Centre of gravity variation, Linear quadratic regulator, Gain scheduling, Cubic spline.

1.Introduction
Characteristic aircraft (A/C) responses during varied flight modes always concern researchers as the A/C dynamics regularly change at altitude (H) and Mach number (M) constraints. The A/C centre of gravity (CG) locations also transit along flight conditions and may cause severe structural vibrations since the CG position is a dominant parameter for the longitudinal characteristics because the gravity vector does not lie in the plane of the lateral flight [1]. The fore-and-aft CG locations affect longitudinal stability and control. The Boeing 747-100 (B747-100) A/C's CG symptomatically lies at 25% mean aerodynamic chord (MAC) (MAC length nearly 32 m from the nose tip) [2].

*Author for correspondence

The CG characteristically shifts from 11% to 33% of a MAC as M and H vary [1]. CG positions have to satisfy flying qualities as payloads alter alongside the flight. The variable CG locations also cause higher-frequency structural vibrations that can degrade the A/C flying qualities and the controller performances [2]. The coupling degree between an airframe and controller dynamics has to be well assessed for stable CG location margins.

Un-modelled CG uncertainties over the flight envelope are a reason for the severity in the stability and control management. A highly authenticated control system that would have to handle the uncertain operations and disturbed parameters should be pursued instead of fixed-gain control applications [3]. Those systems would jeopardise the overall performance and robustness as the system gains vary over the operating conditions. The stability

augmentation system based on fixed controller designs may not qualitatively meet various flight responses. Smoother variations in the controller parameters could make the A/C responses thoroughly satisfied. The gain scheduling (GS) design offers efficient interpolation in-between responses by scheduling the compensator gains. Most scheduling methods need extensive tuning for good robust performance due to a lack of matching with controller design methods [4].

This research is motivated by a given background and the former work [3], where B747-100 longitudinal flight simulations at M-H of 0.2 at sea level, 0.5 at 6096 m, and 0.9 at 12190 m were conducted. An entire state feedback (FSF) and linear quadratic regulator (LQR) algorithm, designated as (FSFLQR), was used to manage longitudinal coupling states with elevator-throttle control. The results highlight that the plane is dynamically stable and satisfactorily trimmed at CG cruise conditions. Because flight data, aerodynamic, and stability derivatives are not obtainable for the M-H conditions, the longitudinal flight simulations could not be achieved for the vast flight cases. Also, it is extremely tough to run too many simulations based on a repetitive design approach. However, a controller could not be globalised for robustly stable flight encountering aerodynamics and stability derivatives' uncertainties as M and H conditions differ along with the longitudinal flight envelope. Hence, the GS method will be imposed with the old FSF-LQR algorithm [3] to achieve promising global control law over the longitudinal flight envelope so that the plane is dynamically stable and satisfactorily trimmed at all CG cruise flights.

This paper investigates the B747-100 longitudinal flight performance over the entire M-H envelope. The GS approach will be applied to visualise the B747-100 longitudinal responses fully. The FSF-LQR algorithm is implemented to obtain optimal longitudinal flight responses at the three baselines trimmed operating conditions at (M, H) of (0.2, 0), (0.5, 6096 m) and (0.9, 12190 m), representing the A/C equilibrium point (EP). The design of efficient control law covering all the flight regimes would be desirably sought. Thus, the extension of these flight points is essential to obtain an approved control law for the longitudinal flight of the B747-100. Cubic spline (CSL) interpolations are used to get the intermediate responses concerning time (t) of axial velocity (u), normal velocity (w), true airspeed (U), pitch rate (q), pitch angle (θ) and time-dependent elevation (h = f(t)). The scheduling variables, which are purposely arranged to be M and H as the flight variables depend thoroughly, are discretised using the Latin hypercube (LHC) design. Then, the angle of attack (α) and flight path angle (γ) are obtained. Local controllers are scheduled at M from 0.2 to 0.9 and H from 0 to 12190 m, so the LQR gains are smoothly driving the entire responses to steady-state levelled convergences in a reasonable simulation time. The proposed synthesis termed GS-FSFLQR healthy verifies the closed-loop specifications with flying handling quality reassurances.

The paper is presented as follows. Section 1 gives an introduction, including background, motivation, objectives, and fulfilments. Section 2 reviews literature. Section 3 shows the procedure covering the longitudinal flight model, LQR algorithm, FSF control law, LHC design, GS algorithm and GS-FSFLQR diagram. Section 4 represents results, including gridded M-H flight envelope, longitudinal response scheduling and CG shift scheduling. Section 5 gives the discussion covering comparative analysis and limitations. Section 6 shows the conclusion and future work.

2.Literature review

The classical GS technique offers exploratory data analysis over a widespread system regime when not enough data is available or to avoid running extensive simulations and/or experimentations [4]. Most GS forms are based on applying a linear approach to the time-varying non-linear models. A single linear time-invariant (LTI) controller is tough to be reached for the entire operating envelope. The classical designs offer a more straightforward GS approach than optimal linear counterparts with relatively high order and complex structures. A robust LTI controller shows some lack in managing un-modelled uncertainty and stability requirements for the entire operating regime [5]. The GS technique has been seen in many successful non-linear control applications such as A/C, missiles, engines, and process control [4]. A collection of LTI approximations is obtained to make an overall fitting design for the non-linear cast at permanent operating conditions. The linear parametrically varying (LPV) system was applied using quadratic stability for the performance analysis of missile autopilot design [6]. In the late 1980s, Rugh [4] used extended linearisation to develop an analytic GS design framework. Shamma and Athans [7] emphasised that the scheduling parameter should gently fluctuate based on LPV. Yue et al. [8] simulated the wing-

hinged mechanism plane using the linear variable variation procedure due to the transforming wing structure and dynamics change in aerodynamic forces and moments. The obtained linearised system validates competently parameter variations manging compared to the non-linear simulations.

High-order polynomial interpolation causes a visible deterioration due to its high sensitivity to data errors [9]. Newton and Lagrange's interpolations deviate considerably from the accurate guess. These formulations require comparable computational effort and are pretty fit for encoding. However, the Newton form requires the space packing of divided differences and the Lagrange algorithm is desired for the polynomial predicated order. These techniques are widely implemented using a divided-difference table. Higher-order polynomials might cause invalid interpolations owing to round-off errors and oscillations. However, lower-order polynomials can be used to subsets of data points in a piecewise fashion. Connecting these polynomials will perform a better interpolation scheme called spline-based functions. Lower-order splines can be used effectively to capture the curving trends of data without suffering from oscillations. However, higher-order polynomial splines are smooth compared with first-order splines. CSL in third-order polynomials is also valid for continuous first and second derivative implementations. The CSL is reportedly ideal for computer implementation. Zhou et al. [10] controlled the fault A/C elevator bomb model using the LPV method based on optimal control and linear matrix inequalities (LMI) approaches. The proved simulations showed another efficacious elevator scheduling parameter for the favourite performance in the case of failures without retuning the controller. The Hayakawa et al. study [11] showed that an observer-based quadratic guaranteed cost controller that merged the LMI was more effective than traditional approaches for system uncertainties and gain variations.

The LQR method was used to control the pitch angle of general aviation A/C for longitudinal cruise flight [12]. It exhibited a good performance when the plant was not corrupted by disturbance. The FSF-LQR algorithm was used to manage longitudinal coupling states with elevator-throttle controls of the B747-100 A/C at (0.2, sea-level), (0.5, 6096 m), and (0.9, 12190 m) of (M, H) representations [3]. The results highlighted that the plane was satisfactorily trimmed at CG cruise conditions. However, the control algorithm could not be generalised to manage the robust performance under uncertain flight conditions. Sir et al. [13] developed fractional-order-integral LQR control (FI-LQR) using the heuristic optimiser. The non-minimum phase was analysed for the pitching-up B747 tracking flight of an altitude-hold system. Their approach showed more robust effectiveness than the FSF and pole placement strategy for fault-free, 50%, and 80% losses of actuator efficiency of flying states. The authors [14] handled the aerodynamics and gyroscopic moments of the dynamic quadcopter system. They used LQR and the Newton-Euler method based on a yaw angle linearisation. The algorithm, incorporated in Simulink, performed well under highly variant yaw attitudes of reference flight paths. However, tracking steady-state errors were highly pronounced in the reference signals, and their weighting matrices did not adequately adapt for various design objectives and the dynamic response. Yang et al. [15] proposed the LQG method for identification based on the Levenberg-Marquardt scheme of tip-tilt disturbance model with little prior information. They found LQG controller capably performed in several adaptive optics systems in replay mode simulation. Co-workers in [16] compared proportional-integral-derivative (PID), proportional-derivative (PD), LQR, proportional LQR (P-LQR), PD-LQR and proportional-derivative-derivative LQR (PD2-LQR) control strategy for the altitude control and attitude stabilisation of quadcopter applications. Almost all the finding flight responses of quadcopter four motions noticeably improved due to the proposed PD2LQR as an alternative controller. Shauqee et al. [17] controlled altitude and attitude responses demonstrated by a quadrotor vehicle. The PD2-LQR was used with an improved grey wolf optimiser (IGWO) to search for an appropriate controller parameter for superior control performance. The tracking quality of the IGWO-PD2LQR was revealed for 20 quadcopter models and outperformed those controllers in [16].

Brizuela-Mendoza et al. [18] controlled a rider-less bicycle by combining the LQR and GS integral controller to manage the bar torque for a vertically stable bike. The experimental report based on the time-varying transitional velocity showed the accurate agreement to stabilised automatic bicycles. Wang et al. [19] suggested the new method of the LQR and GS algorithms based on robustness to un-modelled vehicle yaw moment variables. Such an approach deals with uncertain and disturbing performance and eliminates the tracking error closer to the state-space source. Such a robust LQR (R-

LQR) showed a proven reduction in yaw variable error predictions in comparison with classical LQR control design [3]. Full six degrees of freedom coupled quadcopters were also controlled by Okasha et al. using the LQR method [20]. The varied yaw heading attitude in loop and spiral trajectory was investigated without ranting and discontinuous commands. Arif et al. in 2018 [21] assessed A/C control systems using X-Plane 10, Python and MATLAB. They used simulation system rigs to configure A/C loads and identify possible system failures. The simulation podium showed high compatibility among those software tools. It manipulates the controllability and observability properties of an A/C design system. Bondarenko and Zybin [22] applied the nonparametric failure detection principle to analyse the linear dependence of the input-output Hankel matrix columns for the solution of the sensor ruins localising difficulty shown on the B747−100/200 longitudinal flight. Their proposed algorithm expressed prompt tuning, rapid responsiveness and cautious sensitivity. Saussié et al. [23] successfully benchmarked the new GS approach on a missile autopilot. Guardian GS maps were proposed without designing linear control and interpolating gains over the parameter space. The subjective performance was globalised to the ample space of the linearised gain model.

Welstead and Crouse [24] implemented the lower-order conceptual design tool incorporating varied A/C disciplines, including flight dynamics and LQR constant gains. Such advanced implementation can be used to investigate larger spaces allowing adjusting the design of control surfaces based on dynamic responses. The control allocation method was proposed for conventional trim optimisation formulations of multi-axis control vehicles [25]. Such a technique decreases the variable dependences for curved optimisation formulations, including drag and thrust problems. The method convergence was also refereed based on controlled deflections. Hameed and Bindu [26] integrated an LQR with the GS scheme for the touchdown vehicle merits of approach and landing phases. The application was adequately robust to tackle drag problems during these stages under off-nominal initial conditions. The authors [27] said that using the GS technique based on linearising the non-linear dynamics of a missile autopilot at several trim points would perform well in accurate flight. They suggested a sum-of-squares optimisation algorithm to validate such substantially non-linear characteristics in flight conditions adequately. The closed-loop system performance was verified for short-period and skid-to-turn modes. Colombo and Da [28] found that an adaptive model predictive control (AMPC) outperformed the gain scheduling linear quadratic regulator (GS-LQR) for a flexible manufacturing Cartesian manipulator that comes in configured dynamics dependence, particularly with unlimited actuation bounds' applications. Ilka and Murgovski [29] used a Newton-based GS approach and an output-feedback LQR control for large-scale uncertain LPV systems. These include air and fuelling management of diesel engines, showing more computationally efficient and sub-optimal robustness based on real-world road profile data than gain scheduling proportional-integral-derivative (GS-PID) benchmarks. Obajemu et al. [30] suggested the GS control for fuel-efficient four-dimensional trajectories. That standardises the autopilot autonomous taxi route based on a high-fidelity A/C model. The proposed application showed a reduction capability of up to 11% in the fuel digestion during the B747 taxiing motion.

An overall analysis of the searched literature [3−30] could reveal that several works would have many relevant findings if the researchers incorporated the GS strategy with their controller methods. They missed out on the system parameter variations and model uncertainty problems where their controller designs were not robustly stable enough under various operational conditions. For instance, the works in [5−11] did not match un-modelled uncertainty for the entire operating conditions owing to the use of the LTI, LPV and LMI methods. Also, authors [3, 12−20] used the classical LQR to control general aviation A/C, B747-100, quadcopter and rider-less bicycles for real limited scenarios. Some of those [13, 16−17, 19] proposed the so-called FI-LQR, R-LQR, P-LQR, PD-LQR, PD2-LQR and IGWO-PD2LQR (Modified LQR versions) to ensure the LQR shortcomings not influencing the performance under unstandardised conditions. Shauqee et al. [17] argued that IGWO-PD2LQR showed more pronounced outperformance than the other controllers' responsiveness. Although those obtained responses were based on different 20 models no sufficient guarantee that satisfactory performance might still be accepted over different operating cases as they tested all 20 quadcopters under the same benchmarking conditions. Authors [21−25] alerted that using the pseudo-GS allowed them to achieve some proposing results covering the more expansive design space of their applications. However, no precise control implementation imposed with the GS algorithm was conceptualised. Instead, they

interpolated between the responses to obtain the global gains of the control system. Then, co-workers [18−19, 26−30] succeeded in using the GS in one platform with their control law system (PID, LQR) to manage different applications ranging from the rider-less bicycle, vehicles, A/C, missiles, diesel engines and fuel ingestion during the B747 taxiing. It is shown the efficient capability in handling the variable dependences of large spaces and adjusting the control designs based on dynamic responses. Colombo and Da [28] claimed AMPC overtook GS-LQR for unlimited actuation bounds. However, apparent advantages are seen among the GS-LQR applications for stable systems, good reference tracking performance and controller robustness. To model A/C CG variations over the B747-100 longitudinal flight envelope based on coupling elevator and throttle control parameters, the CG-FSFLQR synthesis was confidently adopted to achieve those objectives.

3.Methods

3.1Longitudinal flight modal

The B747-100 longitudinal flight is actuated using cross-coupled control of the elevator and throttle, where the linearised state-space form can be given by Equation (1). These A/C and control matrices are given by Equation (2) and Equation (3), respectively.

$$\begin{bmatrix}\Delta\dot{u}\\ \Delta\dot{w}\\ \Delta\dot{q}\\ \Delta\dot{\theta}\\ \Delta\,\dot{h}\end{bmatrix} = A\begin{bmatrix}\Delta u\\ \Delta w\\ \Delta q\\ \Delta\theta\\ \Delta h\end{bmatrix} + B\begin{bmatrix}\Delta\delta_e\\ \Delta\delta_t\end{bmatrix} \quad (1)$$

$$A = \begin{bmatrix} X_u & X_w & 0 & -g & 0\\ Z_u & Z_w & u_0 & 0 & 0\\ M_u + M_{\dot{w}}Z_u & M_w + M_{\dot{w}}Z_w & M_q + M_{\dot{w}}u_0 & 0 & 0\\ 0 & 0 & 1 & 0 & 0\\ 0 & -1 & 0 & u_0 & 0\end{bmatrix} \quad (2)$$

$$B = \begin{bmatrix} X_{\delta_e} & X_{\delta_t}\\ Z_{\delta_e} & Z_{\delta_t}\\ M_{\delta_e} + M_{\dot{w}}Z_{\delta_e} & M_{\delta_t} + M_{\dot{w}}Z_{\delta_t}\\ 0 & 0\\ 0 & 0\end{bmatrix} \quad (3)$$

where A is a five × five matrix presenting A/C dynamics and B is a five × two matrix representing control and stability characteristics. They are given in the derivatives of forwarding force (X_u), transverse force (Z_u) and pitching moment (M_u) concerning axial velocity (u). Similarly, the other derivatives of ($X_{\boxdot}$), ($Z_{\boxdot}$) and ($M_{\boxdot}$) are defined concerning normal velocity (w), transverse velocity derivative ($\dot{w}$), pitch rate (q), elevator deflection (δ_e) and throttle actuation (δ_t). u_0 is a steady-state velocity and g is a gravity acceleration (9.81 m/sec^2). Equation (2) and Equation (3) are readily accessed at M and H over the flight space Ɛ(M, H).

Since the thrust-throttle relationship is not linear, the thrust effects were not introduced into the state-space model. Also, the thrust does not exert on the origin of the CG stability axis. Thus, jet engines and throttle actuators were not modelled explicitly in the system model. The engine model simplified the complex analysis due to some lag between the engine servo and the engine [1]. The full-states longitudinal responses can easily be obtained regarding all the states as system outputs. Thus, the response observation matrix and the reference transition matrix were taken as unity and nullity matrices, respectively. The angle of attack and flight path are in sequence, as shown in Equation (4). For the longitudinal flight approximation, the side velocity could be disregarded, and the true airspeed can be composed of axial and normal velocities as given in Equation (5).

$$\left.\begin{aligned}\propto &= \tan^{-1}({}^{w}/_{u}) \cong {}^{w}/_{u}\\ \gamma &= \theta - \propto\end{aligned}\right\} \quad (4)$$

$$U \cong (u^2 + w^2)^{1/2} \quad (5)$$

3.2LQR algorithm

The LQR control law is typically used as well as a state-space method to find the optimal control gains for a large-scale multivariable system. Static gains may be more adequately than time-varying gains for a long time horizon. It also provides significant savings in the implementation of complexity and computational demand. The controller can be tuned by adjusting the state and weighting control matrices, in turn, Q and R. The cost function of the LQR is given by Equation (6) below.

$$J\big(x(t), \delta(t)\big) = \int_0^t [(x^T \mathrm{Q} x) + (\delta^T \mathrm{R}\delta)]dt \quad (6)$$

The first term and the second term of Equation (6) penalise the overall state deviation and control effort, respectively. The control law ensures that J is non-negative and zero for the optimal tracking system.

The state variable vector and the control vector are, in turn, defined by Equation (7) and Equation (8).

$$x = [\Delta u \quad \Delta w \quad \Delta q \quad \Delta\theta \quad \Delta H] \tag{7}$$

$$\delta = [\Delta\delta_e \quad \Delta\delta_t]^T \tag{8}$$

Here, $\mathrm{Q} = \mathrm{Q}^{\mathrm{T}} \geq 0$ is a five × five state weighting matrix and $\mathrm{R} = \mathrm{R}^{\mathrm{T}} > 0$ is a two × two control weighting matrix. t is an unconstrained state/control time primarily defined by the simulation time. The convergence quality of the LQR method depends on state and control variables, which select Q and R. Diagonal Q and R matrices are generally used to decouple specific dynamics [31]. Also, pitch rate and attitude should possess small comparative weighting between the control and states by using Bryson's rules for the initial guesses of Q and R. The assessment of the control algorithm performance may be accurately achieved by defining the objective function underlying the system problem based on various types of integral absolute error (IAE). In the abundance of literature [14−20], integral square error (ISE), integral time absolute error (ITAE), and integral time square error (ITSE) are widely used to optimise those control laws [32]. However, a refined IAE (RIAE) [17], RIAE= $\int_0^{tf} (J(x, \delta) + r_t + O_s + e_{ss})\, dt$ was suggested by accumulating the rise time (r_t), percentage overshoot (O_s), and steady-state error (e_{ss}), merging them with the IAE cost function Equation (6).

3.3FSF control law

The FSF controller strategy has to be designed by choosing a regulator gain matrix (K). The FSF algorithm can linearly combine the longitudinal states if these states are fully feedback as derived from Equation (9).

$$\Delta\delta_e = \mathrm{k_{ue}}\Delta u + \mathrm{k_{we}}\Delta w + \mathrm{k_{qe}}\Delta q + \mathrm{k_{\theta e}}\Delta\theta + \mathrm{k_{he}}\Delta h$$

$$\Delta\delta_t = \mathrm{k_{ut}}\Delta u + \mathrm{k_{wt}}\Delta w + \mathrm{k_{qt}}\Delta q + \mathrm{k_{\theta t}}\Delta\theta + \mathrm{k_{ht}}\Delta h \tag{9}$$

where $\mathrm{k_{ue}}, \mathrm{k_{we}}, \mathrm{k_{qe}}, \mathrm{k_{\theta e}}$ and $\mathrm{k_{he}}$ are regulator gains named axial velocity, normal, pitch rate, pitch angle and height for an elevator, respectively. $\mathrm{k_{ut}}, \mathrm{k_{wt}}, \mathrm{k_{qt}}, \mathrm{k_{\theta t}}$ and $\mathrm{k_{ht}}$ are regulator gains termed axial velocity, normal velocity, pitch rate, pitch angle and height for a throttle, respectively.

The optimal control effort is derived as shown in Equation (10). Thus, Equation (10) demonstrates the state feedback gain, which can be defined by Equation (11). Matrix P is solved using the steady-state algebraic Riccati equation or Equation (12).

$$\delta = -\mathrm{R}^{-1}B^T\mathrm{P}x(t) \tag{10}$$

$$\mathrm{K} = \mathrm{R}^{-1}B^T\mathrm{P} \tag{11}$$

$$-\mathrm{P}A - A^{\mathrm{T}}\mathrm{P} + \mathrm{PBR}^{-1}B^T\mathrm{P} - \mathrm{Q} = 0 \tag{12}$$

Once the optimal LQR gains, K, results in swift longitudinal convergences, the autopilot will take place for effectively tracking purposes. The steady-state limit for the step response can be evaluated by:

$$\lim_{t\to\infty} x(t) = -A^{-1}B\delta \tag{13}$$

Such Equation (13) indicates the initial perturbed responses must die out as $t \to \infty$ to assure the dynamic stability of the A/C system. The state errors are minimised by the autopilot using the state gains, and they were obtained as shown in Equation (14). The elevator and throttle servos were taken constants. The errors in elevator deflection and throttle control which are to be minimised in the inner loop, are defined by Equation (15).

$$\left.\begin{aligned} E_u &= u - u_c \\ E_w &= w - w_c \\ E_q &= q - q_c \\ E_\theta &= \theta - \theta_c \\ E_h &= h - h_c \end{aligned}\right\} \tag{14}$$

$$\left.\begin{aligned} E_{\delta_e} &= \delta_e - \delta_{ec} \\ E_{\delta_t} &= \delta_t - \delta_{tc} \end{aligned}\right\} \tag{15}$$

The command actuation signal is $\delta_c = [\Delta\delta_{ec} \quad \Delta\delta_{tc}]^T$. Once the optimal LQR gains, K, were obtained and fast convergences were reached, the inner loop was no longer needed, and the autopilot on the outer loop took place. The servo constants (servo gearing) were set to obtain practical elevator deflections and throttle commands. For simplicity, the observation matrix (C) of the rate gyro, attitude gyro, potentiometer, altimeter and accelerometer readings were taken to be the identity matrix. *Figure 1* shows the closed-loop control system of longitudinal A/C dynamics. The FSF-LQR controller was incorporated into the inner loop to form a stability augmentation system, and the autopilot design was imposed on the outer loop to compensate the states to the commended states (u_c, w_c, q_c, θ_c and h_c).

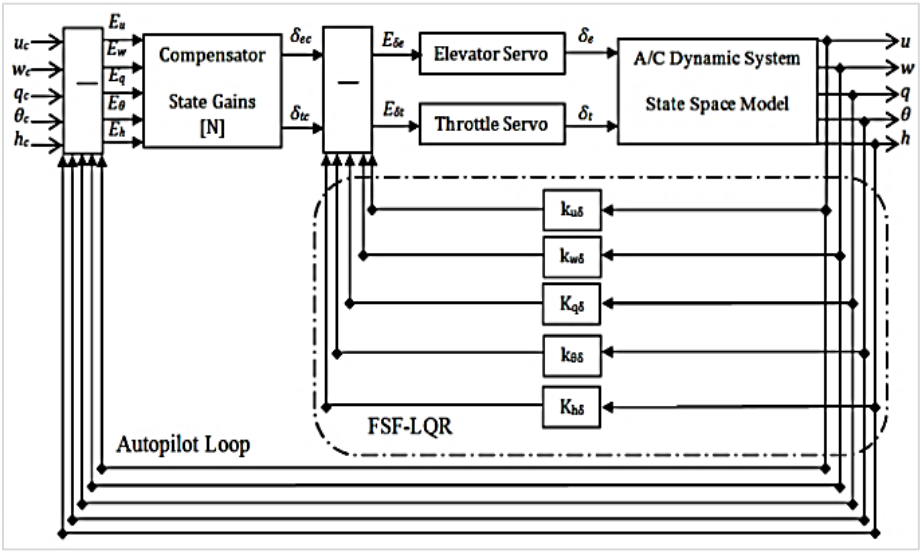

Figure 1 A/C longitudinal dynamics control system

3.4LHC design

The LHC space-filling design was used to avoid the probability of the same design cropping up twice in a sampling plan (M, H) where the size plan (n) was predetermined. A small enough plan was initially used to fit safely into the budget. The following points were selected based on which areas appeared promising. Since the vast budget is highly expansive, the repetitive fitting process is impractical. The possible pairs of points (M, H) may be distant by d_1, d_2, d_3,…, d_n. The number of pairs (M, H) separated by the distance d_j is termed by J_1, J_2, J_3,…, J_n. X is the maximum plan among all available plans if it maximises d_1, d_2, d_3,…, d_n among proper plans in corresponding with minimising J_1, J_2, J_3,…, J_n among plans for which this fact is actual. The Euclidean norm metric of the space can be represented by Equation (16).

$$d_2\left(\mathrm{M}^{(i)}, \mathrm{H}^{(j)}\right) = \left(\sum_1^k \left|\mathrm{M}_k^{(i)} - \mathrm{H}_k^{(j)}\right|^2\right)^{1/2} \qquad (16)$$

A pairwise search through a space design was done based on the scalar-valued criterion function Φ_q as depicted in Equation (17). The smaller value of $\Phi_q\left(\mathrm{M}^{(i)}, \mathrm{H}^{(j)}\right)$ the better space-filling properties of $\left(\mathrm{M}^{(i)}, \mathrm{H}^{(j)}\right)$ is [32]

$$\Phi_q\left(\mathrm{M}^{(i)}, \mathrm{H}^{(j)}\right) = \left(\sum_1^n J_j {d_j}^{-q}\right)^{1/q} \qquad (17)$$

Smaller q was chosen for a more amenable optimised landscape [32]. Sparse populations of M and H databases were considered due to the computational costs of large-scale simulations. Twenty-seven design pairs of M and H were uniformly sampled over the whole design space. The M and H unit mismatches were excluded by scaling these design parameters. Physical design plans were chosen by Equation (18) over $\mathrm{M} \in [0.2, 0.9]$ and $\mathrm{H} \in [0, 12190]$ m.

$$\mathrm{M}^{(i)}, \mathrm{H}^{(j)} = (\mathrm{M}^{(i)}, \mathrm{H}^{(j)}) - (\mathrm{M}_l, \mathrm{H}_l)/(\mathrm{M}_u, \mathrm{H}_u) - (\mathrm{M}_l, \mathrm{H}_l) \qquad (18)$$

where $\mathrm{M_u}$ and $\mathrm{M_l}$ are the higher and minor limits of M, respectively. $\mathrm{H_u}$ and $\mathrm{H_l}$ are the higher and minor limits of H, respectively. i and j are M and H indices (1: n) over the flight design space Ɛ(M, H).

3.5GS algorithm

The one-dimensional interpolations of the longitudinal flight variables will be applied over the discretised flight envelope to produce the LQR gains and state-space models through the nominated intervals. Remarkably, the CSL, which offers a more significant calculation of the possible local abrupt fluctuating behaviour of such longitudinal flight responses, will be used to determine (M and/or H) intermediate responses. Recursive linear functions might obtain the first-order splines of large-scale M points based on Equation (19) and Equation (20).

$$f(\mathrm{M}) = f(\mathrm{M}_i) + m_i(\mathrm{M} - \mathrm{M}_i) \qquad \mathrm{M}_1 \le \mathrm{M} \le \mathrm{M}_n \qquad (19)$$

$$m_i = f(\mathrm{M}_{i+1}) - f(\mathrm{M}_i)/\mathrm{M}_{i+1} - \mathrm{M}_i \qquad (20)$$

Likewise, the first-order splines for large-scale organised H-based data points may be scheduled using recursive linear functions based on Equation (21) and Equation (22).

$$f(\mathrm{H}) = f(\mathrm{H}_i) + m_i(\mathrm{H} - \mathrm{H}_i) \quad \mathrm{H}_1 \le \mathrm{H} \le \mathrm{H}_n \tag{21}$$

$$m_i = f(\mathrm{H}_{i+1}) - f(\mathrm{H}_i)/\mathrm{H}_{i+1} - \mathrm{H}_i \tag{22}$$

However, the CSL in the form of third-order polynomials ensures the continuity of first and second derivatives, which suits practical applications such as flight response interpolations where the meanderings of dynamic longitudinal responses can prettily be captured [9]. A third-order polynomial is typically defined at knots as below.

$$f_i(\mathrm{M},\mathrm{H}) = \alpha_i(\mathrm{M},\mathrm{H})^3 + \beta_i(\mathrm{M},\mathrm{H})^2 + \gamma_i(\mathrm{M},\mathrm{H}) + \delta_i \tag{23}$$

where α, β, γ and δ are variables that can be evaluated by solving the $n-1$ equation. $n-1$ is a simultaneous equation for $n-1$ unknowns at the central knots. The n^{th} equation is now engaged for computation at each interval. Alternatively, the scheme was implemented in MATLAB using built-in functions, which resulted in a more memory-efficient implementation than a lookup table. Thus, a cubic equation will be applied for each interval in terms of M-H subsets:

$$\begin{aligned} f_i(\mathrm{M},\mathrm{H}) = {} & \frac{f_i''(\mathrm{M},\mathrm{H})_{i-1}}{6((\mathrm{M},\mathrm{H})_i - (\mathrm{M},\mathrm{H})_{i-1})}\big((\mathrm{M},\mathrm{H})_i \\ & - (\mathrm{M},\mathrm{H})\big)^3 + \\ & \frac{f_i''(\mathrm{M},\mathrm{H})_i}{6((\mathrm{M},\mathrm{H})_i - (\mathrm{M},\mathrm{H})_{i-1})}\big((\mathrm{M},\mathrm{H}) - (\mathrm{M},\mathrm{H})_{i-1}\big)^3 + \\ & \left[\frac{f_i''(\mathrm{M},\mathrm{H})_{i-1}}{(\mathrm{M},\mathrm{H})_i - (\mathrm{M},\mathrm{H})_{i-1}} - \frac{f_i''(\mathrm{M},\mathrm{H})_{i-1}((\mathrm{M},\mathrm{H})_i - (\mathrm{M},\mathrm{H})_{i-1})}{6}\right] \\ & \big((\mathrm{M},\mathrm{H})_i - (\mathrm{M},\mathrm{H})\big) + \\ & \left[\frac{f(\mathrm{M},\mathrm{H})_i}{(\mathrm{M},\mathrm{H})_i - (\mathrm{M},\mathrm{H})_{i-1}} - \frac{f''(\mathrm{M},\mathrm{H})_i((\mathrm{M},\mathrm{H})_i - (\mathrm{M},\mathrm{H})_{i-1})}{6}\right] \\ & ((\mathrm{M},\mathrm{H}) - (\mathrm{M},\mathrm{H})_{i-1}) \end{aligned} \tag{24}$$

Taking the natural spline conditions are zeros, the remaining second derivatives in Equation (24) are unknowns and are evaluated using Equation (25).

$$\begin{aligned} & ((\mathrm{M},\mathrm{H})_i - (\mathrm{M},\mathrm{H})_{i-1})f''(\mathrm{M},\mathrm{H})_{i-1} \\ & +2((\mathrm{M},\mathrm{H})_{i+1} - (\mathrm{M},\mathrm{H})_{i-1})f''(\mathrm{M},\mathrm{H})_i + \\ & ((\mathrm{M},\mathrm{H})_{i+1} - (\mathrm{M},\mathrm{H})_i)f''(\mathrm{M},\mathrm{H})_{i+1} = \\ & 6/((\mathrm{M},\mathrm{H})_{i+1} - (\mathrm{M},\mathrm{H})_i)\,[f(\mathrm{M},\mathrm{H})_{i+1} - f(\mathrm{M},\mathrm{H})_i] \\ & + 6/((\mathrm{M},\mathrm{H})_i - (\mathrm{M},\mathrm{H})_{i-1})\,[f(\mathrm{M},\mathrm{H})_{i-1} - f(\mathrm{M},\mathrm{H})_i] \end{aligned} \tag{25}$$

3.6GS-FSFLQR diagram

The primary mathematics and algorithms might be concisely illustrated for methodology clarity next. *Figure 2* schematically shows the GS-FSFLQR approach used for the stability and performance augmentations for the B747-100 longitudinal flight over the flight envelope Ɛ(M, H).

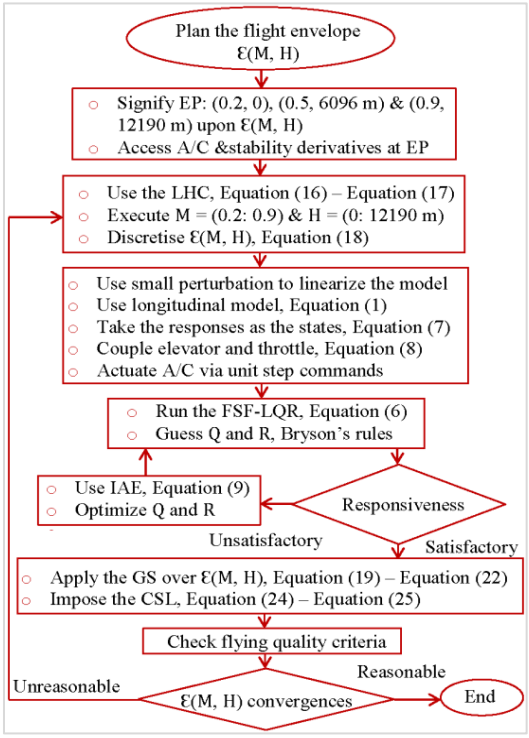

Figure 2 GS-FSFLQR diagram for B747-100 longitudinal flight manoeuvre

The procedure may be briefly illustrated as follows.

1. Planning the longitudinal flight envelope Ɛ(M, H).

2.Retrieving the aerodynamics and control derivatives at EP (0.2, 0), EP (0.5, 6096 m) and EP (0.9, 12190 m) over Ɛ(M, H).

3. Discretising Ɛ(M, H) for M = (0.2: 0.9) and H = (0: 12190 m) using Equation (18) and the LHC based on Equation (16) – Equation (17). ***4.*** Triggering B747-100 A/C based on the longitudinal model as shown in Equation (1) - Equation (8) for small perturbation linearisation and elevator and throttle coupling control by unit step commands. ***5.*** Performing the FSF-LQR for Equation (6) with Q and R Bryson's rules. ***6.*** Investigating the flight responsiveness at EP.

7. Optimising Q and R till reasonable IAE criterion in Equation (9) is achieved. ***8.*** If the flight responsiveness in (***6***) would be satisfactory, the GS over Ɛ(M, H) is applied {Equation (19) – Equation (22)} for not highly fluctuated responses, and the CSL is executed using Equation (24) – Equation (25) so that the links between neighbouring interims looks visually smooth. Both techniques are changeably swapped to cope with the nature of responsiveness meanderings for exact implementations of the GS. ***9.*** Examining flying quality criteria of the longitudinal flight modes. ***10.*** If Ɛ(M, H) convergences are unacceptable, return to (***3***) re-discretising Ɛ(M, H) till reasonable responses are reached; otherwise, terminate for results satisfaction.

4.Results

4.1Gridded M-H flight envelope

The B747-100 longitudinal Ɛ(M, H) in the geometry (M, H) is shown in *Figure 3*. The Ɛ(M, H) boundaries are typically designated as approach, stall, cabin altitude, Mach and dynamic pressure. EP (0.2, 0) and EP (0.9, 12190 m) compatibly target the process and Mach-cabin altitude limits, respectively. However, EP (0.5, 6096 m), which represents the cruise's critical condition, took place almost in the Middle of Ɛ(M, H), surrounded by all these limits.

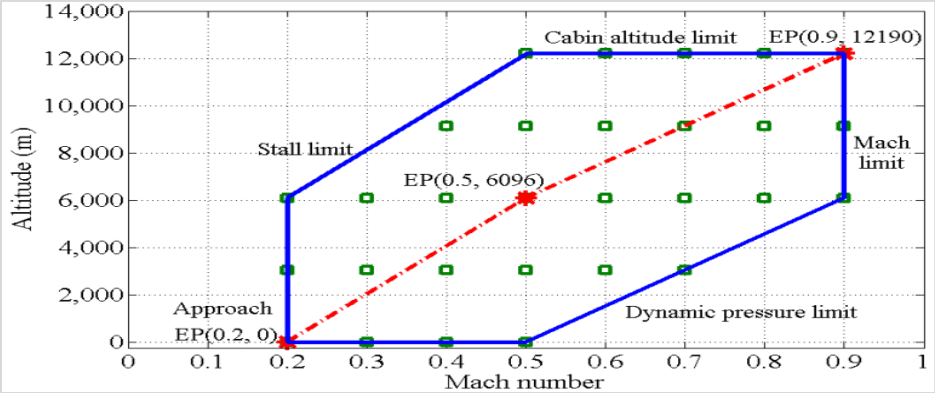

Figure 3 The B747-100 longitudinal Ɛ(M, H) in the geometry (M, H)

The envelope shows the '*g*' loadings at various speeds that A/C withstands. The symmetric manoeuvre is constructed by omitting the effect of side-slipping, rolling or yawing and considering the plane in longitudinal flight under small perturbations in pitching action. A positive-side envelope was mainly identified as a significant part of passenger A/C. The stall speed and cruise speed were chosen to be almost comparable with the A/C design manoeuvring speed based on joint aviation requirements (JAR) and as low as possible to limit the loads on the airframe. The GS control law design can adequately determine the reminder region over the whole flight envelope to perform scaling interpolation based on the EP already obtained from accurate simulations. The control laws are designed locally at some operating points, and the interpolation is made through the scheduling scheme functions. Controller gains are scheduled with some measured parameters of the system. Thus, all the flight and stability derivatives were obtained, and the control law matches the expected flight districts. Such GS implementation ensures the control design is valid for the in-flight stressing cases. The GS design provides acceptable flying qualities inside the operational flight envelope.

Operating points were selected explicitly by the LHC. Operational points were defined with an interval of M = 0.1 and H = 3048 m. The M variables spread from 0.2 to 0.9, and the H parameters are given from sea level to 12190 m. Three red star locations correspond to EP of (0.2, 0), (0.5, 6096 m) and (0.9, 12190 m). These points do not exactly represent the linear variation in in-flight behaviour responses. Then, two divisions were used to have two smoothly linear variations; the first one from (0.2, 0) to (0.5, 6096 m); and the second from (0.5, 6096 m) to (0.9, 12190 m). 9 points are accessible in the first partition and 13 points are available in the second one. In addition, four points are offered along the boundary between the two portions. There will be 29 pins covering widespread regions of the flight envelope. Such divisions require connecting polynomials compatible with the spline application for simple polynomial subsets. Twenty-seven points over the flight envelope were decided to avoid overlapping GS. Also, points were discarded around

the dynamic pressure limit and stall limit regions. Thus, the aeroplane should have acceptable flying quality around the operational envelope for safely manoeuvrable flight.

4.2Longitudinal response scheduling

The B747-100 model was trimmed and linearised on the operating point (H = 6096 m and M = 0.5). The given longitudinal flight model was used to simulate a steady-state cruise flight at (M, H) conditions. Three local linear controllers was constructed at the EP (M, H) of (0.2, 0), (0.5, 6096 m) and (0.9, 12190 m) [3]. The global non-linear controllers were extracted based on scattered operating points over the whole flight envelope and its boundary. Such design has to comply with the performance and handling qualities. The repetitive use of the LQR method was avoided through the interpolation scheme offered by a GS approach. The LQR helped obtain stability augmentation and get converged levelled responses for the baseline cases used by the GS. A discretised M-H flight envelope with 27 (M, H) pairs shown in *Figure 3* was interpolated using the spline technique. The interpolation process was conducted each time based on baseline responses from conducted simulations using the LQR-augmented longitudinal flight model. A/C, control and gain matrices (A, B and K, respectively) were obtained at an intermediate pair. Thus the time responses were found for the whole flight envelope, including the pairs that would not be ready to run full-model simulations because, from one side, it is an expansive approach and, from another side, the scarcity of flight data associated with them.

The interpolated time responses of u, w, q, θ and h states were attained over the M-H envelope. The α and γ time responses were later found from further analysis. Furthermore, the conditions are recognised using thin, dotted, dash-dotted, dash-dot-dashed and thick lines for sea level, 3048 m, 6096 m, 9144 m and 12190 m, respectively. However, Mach numbers are recognised by purple, brown, green, black, blue, and red lines for M = 0.3, 0.4, 0.5, 0.6, 0.7 and 0.8, respectively. Grey lines document M = 0.2 and 0.9 since they are baseline cases obtained directly from the whole simulation. The interpolated responses based on the baseline simulations suggest the LQR controller well handles the complete longitudinal flight envelope. The overall pattern of responses is considerably similar to each other. M and H grid vectors were not strictly monotonic. Thus, increasing the use of the ready build-in MATLAB functions "griddedInterpolant" would produce an unaffordable error. Such a function would not be valid for interpolation. Spline interpolation was adopted to handle such strictly non-monotonic increasing of both M and H vectors. The resultant velocity responses at scheduled flight conditions are shown in *Figure 4*, where true airspeed arrays over M-H flight envelopes are given. Velocities at all the middle conditions met good respect to steady-state values within a reasonable time of less than 60 sec. *Figure 5*, a zooming-in view of *Figure 4*, shows no rugged peaks at the transitory periods for all the interpolated cases. Apart from sea level and M = 0.2, which converged in a few seconds, the other conditions took longer to be converged at a low M compared with a high one, whatever H was. Normal velocity and axial velocity arrays over the M-H flight envelope are, in turn, exposed in *Figures 6* and *7*, and the true airspeed is the resultant velocity obtained from normal and axial velocities. A zooming-in normal speed from 20 sec to 300 sec is also given to show peaks at the transient periods for all the interpolated cases.

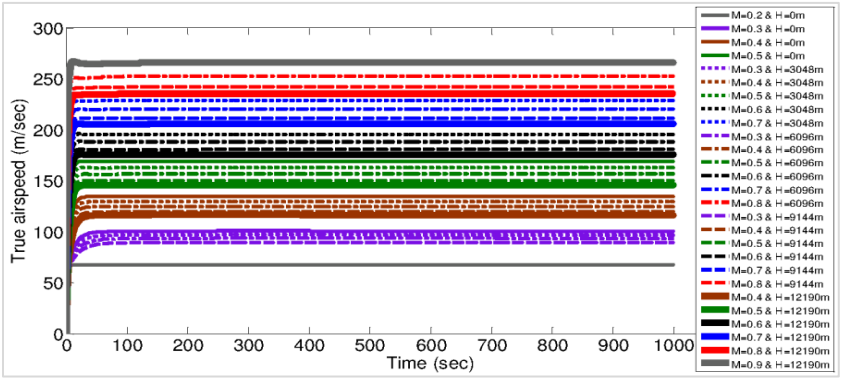

Figure 4 True airspeed arrays over M-H flight envelope

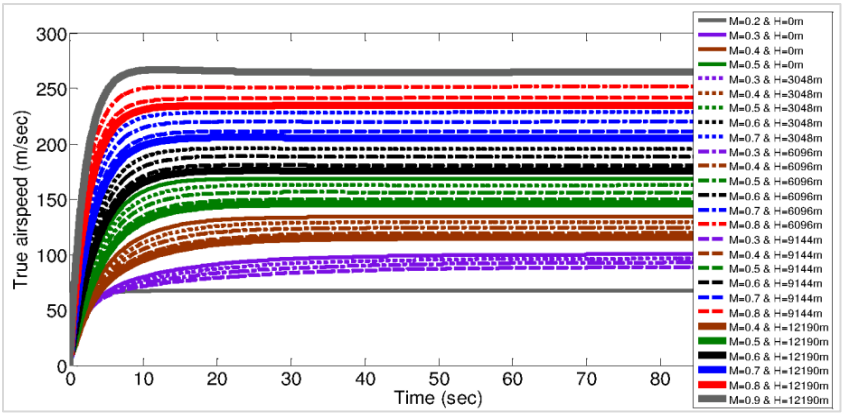

Figure 5 Zoom-in true airspeed arrays over M-H flight envelope

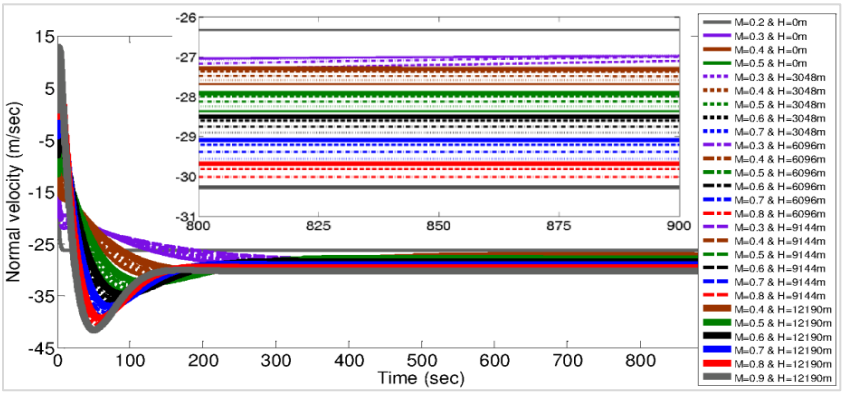

Figure 6 Normal velocity arrays over M-H flight envelope

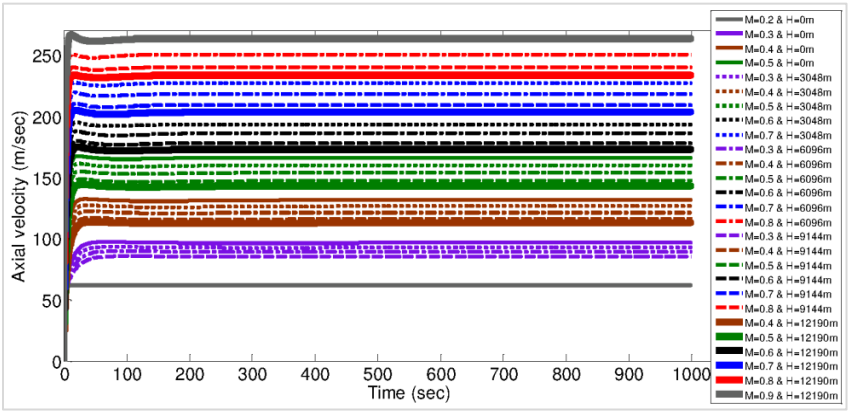

Figure 7 Axial velocity arrays over M-H flight envelope

The altitude-hold arrays over the M-H flight envelope are given in *Figure 8*. Analogous to the true airspeeds, height responses took from about 600 sec to 200 sec to converge as the H got high. However, the cases at sea level & M = 0.2 and 12190 m & M = 0.9 converge in order of 200 sec. Considerably small overshoots, less than three per cent, were found at high altitudes. Pitch rate arrays over the M-H flight envelope are shown in *Figure 9*. A zooming-in view is given at 20-300 sec. Although the convergences took longer to settle, almost zero pitch rate convergences were obtained in the range of 0.002 to -0.004 rad/sec as the merits of longitudinal straight flight. However, the responses were tipped for a high H of about 50 sec at transient regions.

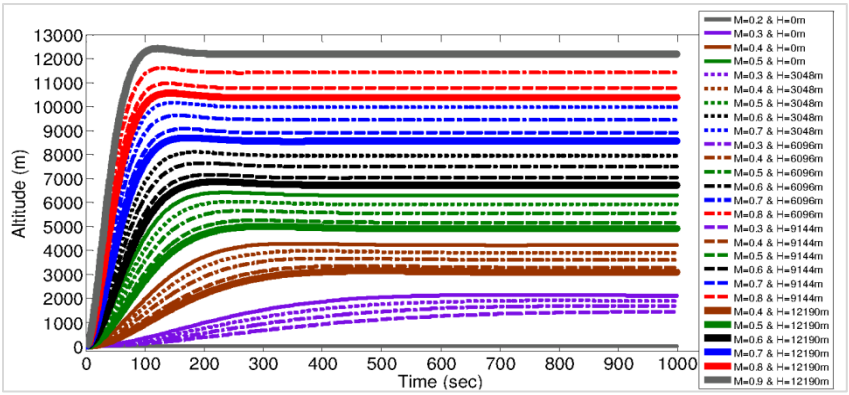

Figure 8 Altitude arrays over M-H flight envelope

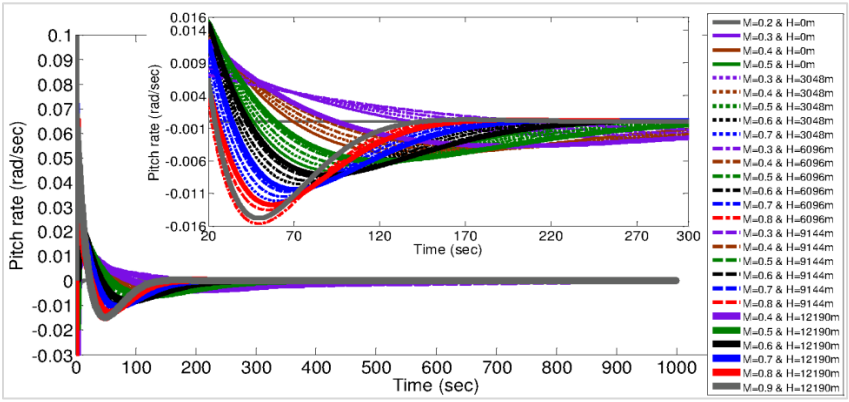

Figure 9 Pitch rate arrays over M-H flight envelope

Pitch angle arrays over the M-H flight envelope are shown in *Figure 10*. Again, as the responses are too close, a zooming-in view is also given at 0-300 sec. The convergences took longer to relax at a range from almost -0.12 to -0.38 rad (-8 deg. to -22 deg.). Also, the responses were tipped for high H and lasted for about 150 sec in transitory regions. Moreover, such a significant change in pitch angles may not change the speed of A/C under-seen circumstances. As observed on the pitch rate, the pitch attitude behaves similarly since the pitch rate is the differentiation of pitch angle. This case pointed out that A/C would be in a cruise pitching with a nose-down because the elevator deflected up. However, the B747-100 trims at the range of -0.234 rad (-13.5°) to 0.069 rad (4°) [10].

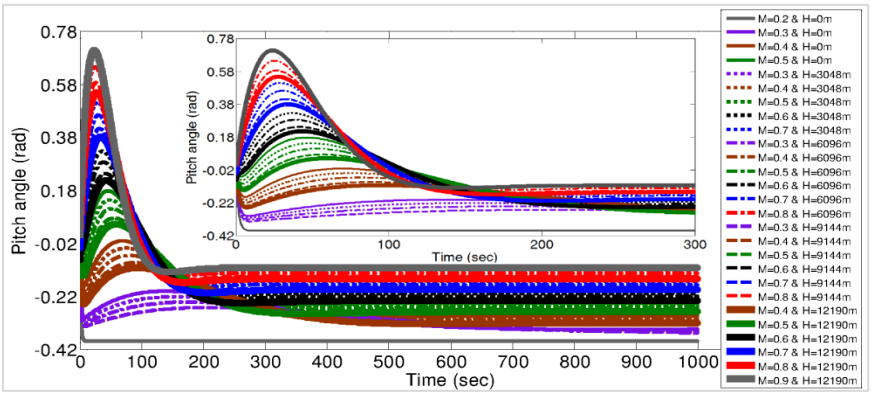

Figure 10 Pitch angle arrays over M-H flight envelope

The angle of attack arrays over the M-H flight envelope is shown in *Figure 11*. The convergences took longer to relax, almost -0.124 rad to -0.425 rad (-6.8 deg. to -24.3 deg.). Also, the spiky responses were observed apart from sea level and lasted for about 150 sec in transient regions. Flightpath angle arrays over the M-H flight envelope are shown in *Figure 12*. The flight path angle responses stemmed from the θ state and α state. A closed-up assessment is also given at 0-200 sec. The convergences took longer to relax at a range from almost 0.04 rad to -0.094 rad (2.29 deg. to -5.38 deg.). Pointed responses still appear apart from the sea level condition and lasted for about 150 sec in transitory regions.

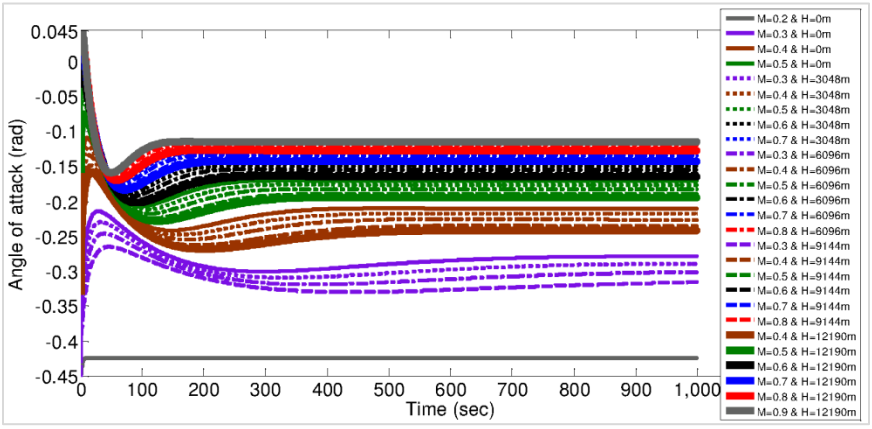

Figure 11 Angle of attack arrays over M-H flight envelope

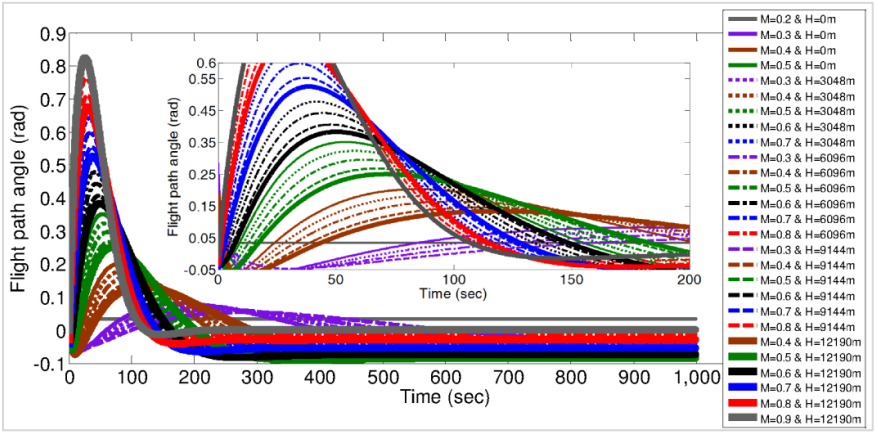

Figure 12 Flightpath angle arrays over M-H flight envelope

4.3CG shift scheduling

As the plane is flown along with the flight envelope, the CG position thus changes from one longitudinal flight position to another. During that, dynamic stability is influenced by coupling elevator and throttle control actions on a longitudinal mission. Along with the M-H flight envelope, not all the CG shifts for the B747-100 were available to carry out the analysis. Moreover, since the B747-100 has a compatible dynamic model with the B747s [33], the B747-400 baseline CG shifts [34] were adopted here. The CG locations were worked out from the plane nose knowing the B747-100 length of 70.7 m. The CG shifts from 11% to 13% MAC within approach flight when the plane tanks got nearly the most petite storage of Kerosene. The B747-100 mean chord is 8.3241 m, and the designed static stability of CG location is likely at 31.8352 m [2]. CG arrays are obtained by the thin plate spline interpolation scheduled over the M-H flight envelope. The baseline CG position at M = 0.2 and sea level was taken at a 12% MAC in which the elevator and throttle were excited to 0.25 rad (14.32°) and 0.23 rad (13.17°), respectively. The baseline CG position of M = 0.5 at 6096 m was assumed at a 26% MAC in which the elevator and throttle were excited to 0.31 rad (17.76°) and 0.58 rad (33.2°), respectively. The baseline CG position of M = 0.9 at 12190 m was adopted at a 25%

MAC in which the elevator and throttle were excited to 0.245 rad (14.04°) and 0.41 rad (23.49°), respectively. *Figure 13 and Figure 14* show the MAC percentage of CG location for the B747-100 longitudinal flight under the influence of elevator and throttle actions, respectively. The throttle deflection is shown in radian for compatibility with the elevator for applying the GS interpolation process. The elevator and throttle deflection data are shown as stems from the CG axis terminated with circles, squares, triangles, diamonds, plus symbols for H = 0 m, 3048 m, 6096 m, 9144 m and 12190 m, respectively. The accompanying Mach numbers are differentiated by colours based on the CG locations by giving the same colour at the same CG position.

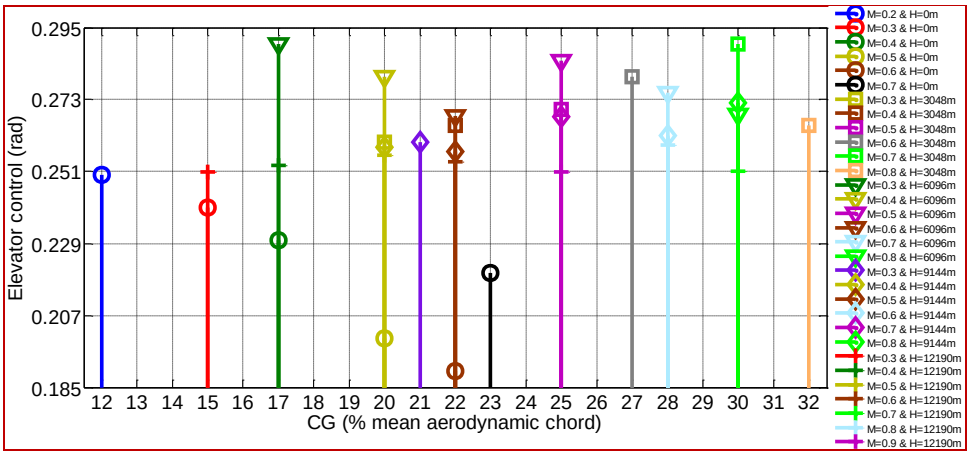

Figure 13 M-H stems of CG MAC% based on elevator control

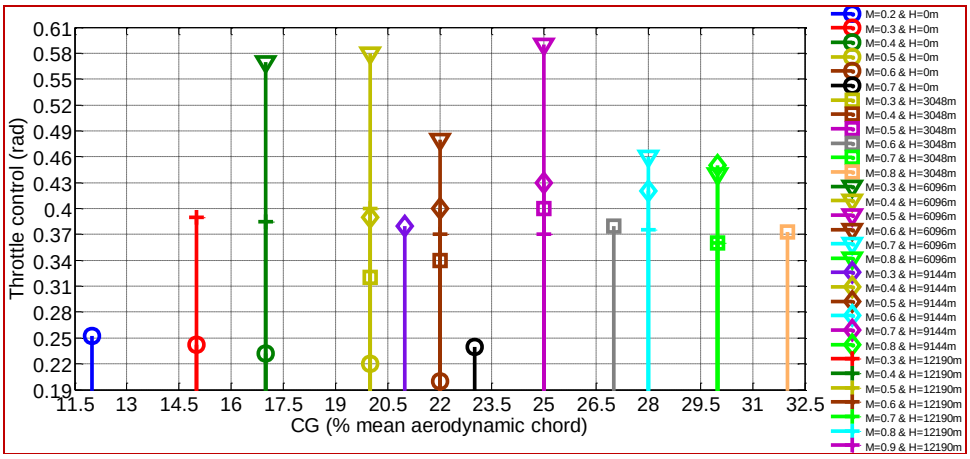

Figure 14 M-H stems of CG MAC% based on throttle control

There is a fluctuation of CG locations as M-H pairs vary, which is correlated with an elevator action. The CG position was 25% MAC (31.8352 m) along trimmed cruise flight of (0.5, 3048 m), (0.5, 6096 m), (0.7, 9144 m) and (0.9, 12190 m). However, the highest elevator power pushes CG to the 17% location at (0.3, 6096 m) and 30% at (0.7, 3048 m) and the lowest is at 22% location for (0.6, sea level). However, most CG locations are fore than 25% MAC for a range of M-H conditions. Overall, the CG position fluctuated from 11% to 17% MAC at M < 0.4 with any H. There is a fluctuation of CG locations as M-H pairs vary, which is correlated with the management of throttle actions. The CG position was 25% MAC along trimmed cruise flight (0.5, 3048 m), (0.5, 6096 m), (0.7, 9144 m) and (0.9, 12190 m). However, the highest throttle power at the 25% CG location is shown for (0.5, 6096 m), and the lowest throttle operation was in consent with the minimum elevator feature. However, the aft and fore CG locations glide around 25% MAC for the other M-H conditions. Again, the CG position fluctuated from 11% to 17% MAC at M < 0.4 with all the H. *Figure 15* shows actuator effectiveness of control actions for

the CG management in terms of the three-dimensional response surface of the elevator and throttle control actions. Almost the effectiveness of these control actions could be correlated to the A/C actuators in longitudinal flight. Such effectiveness might be going to be lost for any combinations of control actions, $\Delta\delta_e$ = {(0.198: 0.28) & (0.23: 0.29) & (0.19: 0.21)} rad and $\Delta\delta_t$ = {(0.35: 0.58) & (0.28: 0.31) & (0.2: 0.6)} rad, representing the blue and red regions. The most effective action of actuators is expected around the green regions and adjacent turquoise regions for the CG shifting about 11% MAC – 32% MAC. ($\Delta\delta_e$, $\Delta\delta_t$) = {(0.26: 0.29), (0.175: 0.25)} rad indicates the under-actuated A/C system, whereas ($\Delta\delta_e$, $\Delta\delta_t$) = {(0.19: 0.21), (0.51: 0.6)} rad indicates the over-actuated control setup. The actuator was modelled to meet the practical elevator position limit of -19º (-0.33 rad) to 16º (0.28 rad) [35].

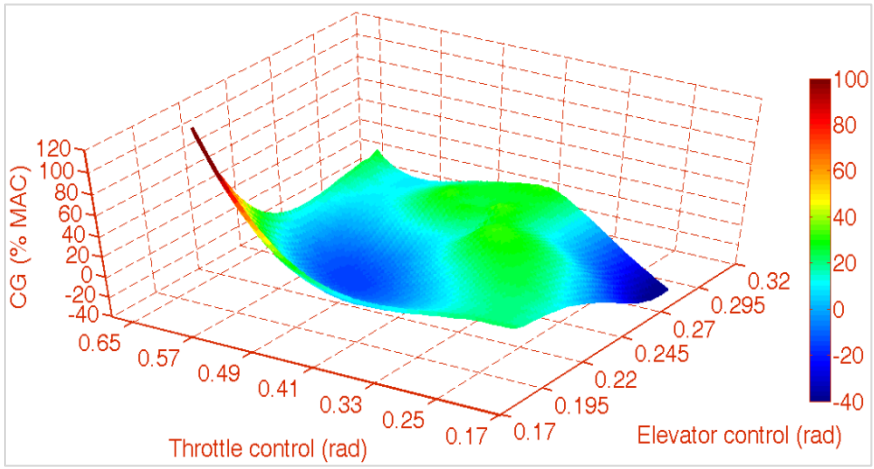

Figure 15 Effectiveness of actuator control actions for the CG management

5.Discussion

5.1Comparative analysis

The GS algorithm would not be susceptible to the linearization made at the equilibrium conditions of (M, H) = {(0.2, 0): (0.5, 6096): (0.9, 12190)}. Since these flight conditions represent the most extreme performance that would be faced when the flaps retracted and the gears up during the B747-100 flight. As shown in *Figure 3*, the first operating condition (0.2, 0) is the approach flight phase in which most landing accidents would have occurred. The middle operating point (0.5, 6096 m) is the critical region around the stall and Mach limits. The third operating point (0.9, 12190 m) represents the cabin altitude limit beyond which the plane would have collided. The findings would be more impressive if the flight data at the EP of dynamic pressure limit, stall limit, Mach number limit and M = 0.5 cabin altitude limit were accessible during the linearisation task. The stall and cruise speeds are diminished based on the JAR requirements to limit the loads on the airframe.

As long as the local LQR controllers exhibit outstanding performances under severe linearising conditions and gain matrices, the uncertainty effects due to varying M and H states and the associated derivatives would be managed by the approach. The servo constants were set for practical elevator deflections and throttled commands, as already depicted in *Figure 13* and *Figure 14*, respectively. Thus, the generalised control law, appreciatively obtained by the GS approach in terms of spline interpolations of the longitudinal flight responses over the flight envelope, is the optimal way to account for such flying uncertainty parameters. However, the conventional pole placement method is highly trivial and awkward for optimal trade-off solutions. Therefore, the synthesis of the GS- LQR algorithm provides significant savings in the implementation of complexity and computational demand. If the *J* of LQR control law asymptotically would approach negative or zero, the EP must be discarded for the algorithm workflow. Moreover, another discretisation attempt has to replace the nonsense point for the best tracking system to be accomplished.

The pitch rate and pitch attitude in longitudinal levelled trim flight should be significantly low with moderately weighting between the control and state matrices. Most simulations were adequate based on the implemented synthesis for longitudinal modes

modelling of the B747 flight, as shown in *Figures 4* to *12*. No severe peaks were found at the transient periods for all the interpolated cases, apart from some conditions that took longer to converge at low Mach numbers compared with high ones for all the H. Also, moderate peaks were seen at the transient periods for all the interpolated cases of pitch rate and heights that are minor states in levelled trim flight. It has ensured that a significant change in pitch angles does not alter the speed of an A/C under the seen circumstance. As the pitch rate is the differentiation of pitch angle, there is no surprise that the pitch attitude behaves in similar patterns to the pitch rate for a cruise pitching with the nose down due to the elevator deflected up. However, the B747-100 trims at the range of -0.234 rad (-13.5°) to 0.069 rad (4°) [33]. The B747-400 baseline CG shifts were advocated for the B747-100 CG compatibility. The CG location is expected at nearly 31.84 m for static stability. The 11%-13% CG shifts indicate the plane tanks got the minor kerosene storage practically at the approach. Because the lag in time constant ratio of throttle to elevator ranges from 15 to 35 [1], the elevator power system responds slower than throttle power to handle some CG variations. Overall, the CG position met 25% MAC along (0.5, 3048 m), (0.5, 6096 m), (0.7, 9144 m) and (0.9, 12190 m), and at which the highest throttle power is obtained at (0.5, 6096 m) and the lowest is at (0.9, 12190 m). Their aft and fore CG locations glide around 25% MAC for the other M-H conditions obeying the handling qualities.

In conjunction with *Figure 15*, satisfactory and acceptable effectiveness regions of actuators are depicted in *Figure 16* for the CG supervision exposed by the legend from -40% to 100% MAC. The contours on the upper right corner represent the under-actuated control setup, whereas these on the lower-left corner signify the over-actuated A/C system. However, the boundary of satisfactory effectiveness region for green contour is not well established to precisely correlate with the actuator values due to the model constraints based on $\Delta\delta_e$ and $\Delta\delta_t$. Nevertheless, the effectiveness loss is clearly exposed over the other contours. The applied approach is more robustly practical than the FSF and pole placement method [13] for 50% actuation operation. No apparent advantages of the GS-FSFLQR over the FI-LQR [13] for the total of 50% efficiency loss as 20% over-actuated and 30% under-actuated in an operable elevator in parallel with 29% over-actuated and 21% under-actuated in an operable throttle. Overall, the flight characteristics are appropriately maintained by varying the CG locations based on the joining actuation setup, which [36] also recapped for fighter A/C using linear quadratic regulator-linear matrix inequalities (LQR-LMI) design.

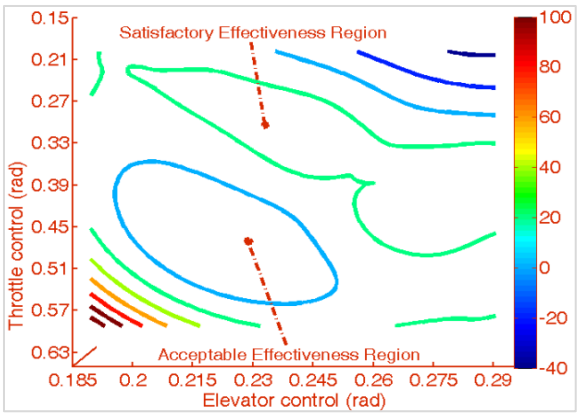

Figure 16 Satisfactory and acceptable effectiveness regions of actuators

Figure 17 compares the pitch rate convergences of the GS-FFLQR with various control implementations [1] and flight tests [35]. Those tests performed rapid pulse in nose-up-down pitching controls to achieve a short-period response [35] compared with the step inputs used in the FSF-LQR. The flight conditions of (M, H) = (0.5, 6096 m) and (0.9, 12190 m) are benchmarked with such findings [1, 36]. These control implementations are based on pole placement, phase advance feedback and blended feedback controls [1]. The latter was commonly used to fulfilling flying qualities throughout the flight envelope. Normalisations were applied to match among plots and exclude discrepancies due to erroneous setups. The Pitch rates were normalised by their mean values, whereas time epochs were normalised by the cycling period. Overall, similar responsive tendencies may be recognised and converged to almost zero for all the cases. It seems comparable damping effects were added to the short period responses. The controls [1] only used elevator action compared with this work applied coupling elevator and throttle actions.

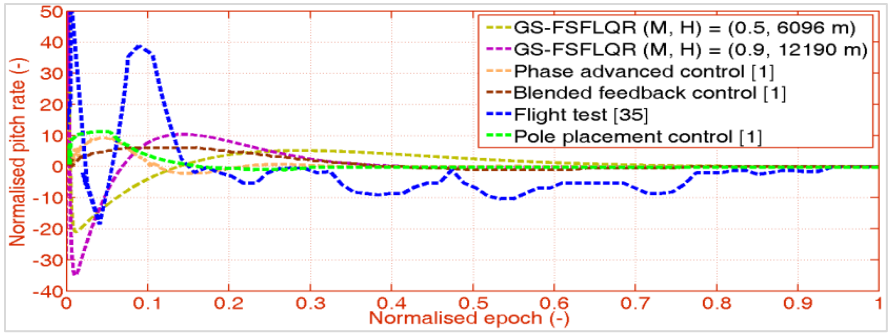

Figure 17 Comparisons of pitch rate convergences with different control implementations and flight test

5.2Limitations

The Q state and R control weighing matrices must not be singular for the desirable convergence quality of the LQR method. Their initial guesses made by Bryson's rule are significant for practical LQR convergences, and the diagonal property has to be matched for coupling system states [31]. It should be emphasised that the RIAE plays a vital role in qualitatively achieving proper state responses, provided that r_t < 500 sec and O_s < 7% to allow wide state responsiveness convergences, including the most severe cases over the flight space Ɛ(M, H). The FSF validity of the LQR application is provided that the states are fully feedbacked and linearly combined, as expressed in Equation (9). The first perturbations Equation (13) must quickly disappear for the A/C dynamic stability. However, the e_{ss} (Equation (9)) was driven to almost zero based on Equation (13) of the FSF as partner implementation to the LQR. The built-in MATLAB functions are more memory-efficient than a lookup table. The GS execution produces accurate trends for the sampling plan of the LHC given in *Figure 3* by changeably incorporating the linear polynomials and the CSL when most spiky responses are experienced. Twenty-seven flight envelope points were used to avoid overlapping the scheduled responses by discarding points nearby the dynamic pressure limit and stall limit regions. The LHC method would fill space effectively if a small enough plan were firstly used to fit safely into the budget. The following points were selected based on which areas appeared promising. Since the vast budget is exceptionally expansive, the repetitive fitting process is impractical.

The non-linear nature of thrust and throttle control is not demonstrated in the state space model. Such a complex relationship is assumed to be linear, considering the thrust does not exert on the origin of the CG stability axis and a bit lag between the engine and its servo [1, 2]. The elevator position was limited from -19º to 16º, which applies to most large transport A/C and its actuator modelling [35]. The output variables are assumed full-states longitudinal responses that exclude the elevator and throttle control coupling effects. Thus, the output observation matrix and the state transition matrix were taken as unity and nullity matrices, respectively. The elevator and throttle servos were assumed constants. The output observation matrix, which represents the altimeter, accelerometer, rate gyro, attitude gyro, and potentiometer readings, is not accessible for benchmarking with realistic A/C and the model here. α and γ states are defined in Equation (4) for small normal velocity. The true airspeed Equation (5) is only computed from axial and normal velocities without the side velocity. Equation (6) of the LQR was optimised for longitudinal states and coupling control actions so that RIAE compactly converges for reasonable O_s and r_t design parameters over the studied M-H envelope. Equation (13) of the FSF delivers e_{ss} to minimal responsiveness, which overall made the RIAE offers the optimal solutions.

6.Conclusion and future work

The feature of the GS approach has been shown in offering a universal controller for the whole B747-100 longitudinal flight regimes. As a result of the aerodynamic and stability derivatives being unmanageable throughout the flight, additional flight data is demanded to tackle those missing and schedule them for an approved control law over the entire flight space. Therefore, the GS technique in interpolations is used to obtain intermediate responses. The FSF-LQR coupling elevator and throttle control have been tested and showed good converged responses as to what the scheduling flight regime should be. The simulation results based on the GS-FSFLQR are coherent regarding good tracking properties of negligible overshoots and steady-state errors.

A feasible control law has been obtained for a range of M and H covering the whole flight envelope. Intermediate trainset responses of velocity, pitch rate, pitch angle and height healthily match the closed-loop performance specifications. The baseline longitudinal flight simulations feed up the GS interpolation at (M, H) = (0.2, 0), (0.5, 6096 m) and (0.9, 12190 m). Local controllers are scheduled at 0.2 to 0.9 for M and 0 to 12190 m for H scheduling parameters. Such linearised controllers drive the responses to smoothly steady-state levelled convergences in a nearly similar manner to each other, which imply how the GS method is successfully implemented. The GS law shows that the coupling elevator and throttle control can competently participate in the CG management during B747-100 longitudinal controlled flight, and those inapplicable couplings have been standard. The CG shifts have also been identified alongside the M-H envelope, placing restrictions on the fore-and-aft CG distributions for permissive flying handling qualities based on the ratio of phugoid frequency to the short-period frequency being higher than 0.1 and the damping between 0.3-2. Overall, the practicality of CG movements is shown for the B747-100 A/C characteristic over the entire flight regime, which has also been correlated with the critical control limits to avoid near-term entry into actuator loss.

The bilinear interpolations will be applied for the global steady-state responses for vast M-H manoeuvres. Modelling the wind gust can also be achieved by alleviation load to peace passenger ride and reducing structural dynamic deformations. For the non-linear simulation, implementing large amplitude could be advantageous for advanced analysis of the actuator losses too.

Acknowledgment

Thanks to the University of Tripoli for the support and the subsidy under Grand 2018. The MTRC Coventry University is also acknowledged for previous supportive consultations.

Conflicts of interest

The authors have no conflicts of interest to declare.

Author's contribution statement

Ezzeddin M. Elarbi: Conceptualisation, investigation on challenges, conducting simulations, data analysis and writing-original draft. **Dina S. Laila:** Proof of the methodology, result interpretations, proofreading, supervision and revision of the draft. **Nadjim M. Horri:** Overall evaluation, supervision and proof of the manuscript.

References

[1] McLean D. Automatic flight control systems. Measurement and Control. 2003; 36(6):172-5.

[2] Etkin B. Dynamics of atmospheric flight. Courier Corporation; 2012.

[3] Elarbi EM, Laila DS, Ghmmam AA, Horri N. LQR reference tracking control of boeing 747-100 Longitudinal Dynamics with CG shifts. In international conference on advanced technology & sciences 2017 (pp. 114-24).

[4] Rugh WJ. Analytical framework for gain scheduling. In American control conference 1990 (pp. 1688-94). IEEE.

[5] Khammash M, Zou L, Almquist JA, Van Der Linden CA. Robust aircraft pitch-axis control under weight and center of gravity uncertainty. In proceedings of the 38th IEEE conference on decision and control (Cat. No. 99CH36304) 1999 (pp. 1970-5). IEEE.

[6] Tan W, Packard AK, Balas GJ. Quasi-LPV modeling and LPV control of a generic missile. In proceedings of the 2000 American control conference. ACC (IEEE Cat. No. 00CH36334) 2000 (pp. 3692-6). IEEE.

[7] Shamma JS, Athans M. Guaranteed properties of gain scheduled control for linear parameter-varying plants. Automatica. 1991; 27(3):559-64.

[8] Yue T, Wang L, Ai J. Longitudinal linear parameter varying modeling and simulation of morphing aircraft. Journal of Aircraft. 2013; 50(6):1673-81.

[9] Griffiths DV, Smith IM. Numerical methods for engineers. CRC Press; 2006.

[10] Zhou Z, Wang X, Wang S, Zhang Y, Gavrilov AI, Nagamune R. LPV active fault-tolerant control strategy of large civil aircraft under elevator failures. In CSAA/IET international conference on aircraft utility systems (AUS 2020) 2020 (pp. 976-981). IET.

[11] Hayakawa S, Hoshi Y, Oya H. Observer-based quadratic guaranteed cost control for linear uncertain systems with control gain variation. Advances in Technology Innovation. 2022; 7:155-168.

[12] Shaji J, Aswin RB. Pitch control of aircraft using LQR & LQG control. International Journal of Advanced Research in Electrical, Electronics and Instrumentation Engineering, IJAREEIE,(An ISO 3297: 2007 Certified Organisation). 2015; 4(8).

[13] Sir EA, Engin SN, Pasha AA, Rahman MM, Pillai SN. Robust control for non-minimum phase systems with actuator faults: application to aircraft longitudinal flight control. Applied Sciences. 2021; 11(24):11705.

[14] Islam M, Okasha M, Idres MM. Dynamics and control of quadcopter using linear model predictive control approach. In IOP conference series: materials science and engineering 2017 (p. 012007). IOP Publishing.

[15] Yang K, Yang P, Wang S, Dong L, Xu B. Tip-tilt disturbance model identification based on non-linear least squares fitting for Linear Quadratic Gaussian control. Optics Communications. 2018; 415:31-8.

[16] Shauqee MN, Rajendran P, Suhadis NM. An effective proportional-double derivative-linear quadratic regulator controller for quadcopter attitude and altitude control. Automatika: a magazine for

automation, measurement, electronics, computing and communications. 2021; 62(3-4):415-33.
[17] Shauqee MN, Rajendran P, Suhadis NM. Proportional double derivative linear quadratic regulator controller using improvised grey wolf optimization technique to control quadcopter. Applied Sciences. 2021; 11(6):2699.
[18] Brizuela-Mendoza JA, Astorga-Zaragoza CM, Zavala-Río A, Canales-Abarca F, Martínez-García M. Gain-scheduled linear quadratic regulator applied to the stabilization of a riderless bicycle. Proceedings of the Institution of Mechanical Engineers, Part I: Journal of Systems and Control Engineering. 2017; 231(8):669-82.
[19] Wang Z, Montanaro U, Fallah S, Sorniotti A, Lenzo B. A gain scheduled robust linear quadratic regulator for vehicle direct yaw moment control. Mechatronics. 2018; 51:31-45.
[20] Okasha M, Shah J, Fauzi W, Hanouf Z. Gain scheduled linear quadratic control for quadcopter. In IOP conference series: materials science and engineering 2017 (p. 012009). IOP Publishing.
[21] Arif A, Stepen A, Sasongko RA. Numerical simulation platform for a generic aircraft flight dynamic simulation. International Journal of Engineering and Technology. 2018; 7(4):53-61.
[22] Bondarenko YuV, Zybin EY. Functional control of the technical condition method for aircraft control system sensors under complete parametric uncertainty. Scientific Bulletin of the Moscow State Technical University of Civil Aviation. 2020; 23(3):39-51.
[23] Saussie D, Saydy L, Akhrif O. Gain scheduling control design for a pitch-axis missile autopilot. In AIAA guidance, navigation and control conference and exhibit 2008 (p. 7000).
[24] Welstead J, Crouse GL. Conceptual design optimization of an augmented stability aircraft incorporating dynamic response and actuator constraints. In 52nd aerospace sciences meeting 2014 (p. 0187).
[25] Garmendia DC, Mavris DN. Alternative trim analysis formulations for vehicles with redundant multi-axis control surfaces. Journal of Aircraft. 2016; 53(1):60-72.
[26] Hameed AS, Bindu GR. Gain scheduled finite horizon LQR for approach and landing phase of a reusable launch vehicle. Journal of The Institution of Engineers (India): Series C. 2022:1-8.
[27] Seo MW, Kwon HH, Choi HL. Sum-of-squares-based region of attraction analysis for gain-scheduled three-loop autopilot. International Journal of Aeronautical and Space Sciences. 2018; 19(1):196-207.
[28] Colombo FT, Da SMM. A comparison between gain-scheduling linear quadratic regulator and model predictive control for a manipulator with flexible components. Proceedings of the Institution of Mechanical Engineers, Part I: Journal of Systems and Control Engineering. 2022:09596518221087805.
[29] Ilka A, Murgovski N. A computationally efficient approach for robust gain-scheduled output-feedback LQR design for large-scale systems. IFAC-PapersOnLine. 2020; 53(2):5988-93.
[30] Obajemu O, Mahfouf M, Maiyar LM, Al-Hindi A, Weiszer M, Chen J. Real-time four-dimensional trajectory generation based on gain-scheduling control and a high-fidelity aircraft model. Engineering. 2021; 7(4):495-506.
[31] Shinners SM. Modern control system theory and design. John Wiley & Sons; 1998.
[32] Sobester A, Forrester A, Keane A. Engineering design via surrogate modelling: a practical guide. John Wiley & Sons; 2008.
[33] Tipps DO, Skinn DA, Rustenburg JW, Jones T, Harris DA. Statistical loads data for the Boeing 777-200ER aircraft in commercial operations. Federal Aviation Administration William J. Hughes Technical Center AR-06/11, Atlantic City, NJ. 2006.
[34] Blight JD, Gangsaas D, Richardson TM. Control law synthesis for an airplane with relaxed static stability. Journal of Guidance, Control, and Dynamics. 1986; 9(5):546-54.
[35] Raol JR, Singh J. Flight mechanics modeling and analysis. CRC Press; 2008.
[36] Nepomuceno L, Moura ÉA, Morales MA, Silva RG, Góes LC. An LQR-LMI longitudinal stability augmentation system for a subscale fighter aircraft with variable center of gravity position. In AIAA AVIATION 2022 Forum 2022 (p. 4059).

Ezzeddin M. Elarbi was born in Tripoli, Libya, in 1976. He received a B.Sc. degree in Aeronautical Engineering from Tripoli University, Aeronautical Engineering Department, the first-class honour, in 2000 and the Aeronautical Engineering Diploma from the University of Tripoli, the first-class honour, in 2003. He got an M.Sc. degree in control systems from the University of Sheffield, with distinction, in 2006 and obtained a PhD from the University of Sheffield, Mechanical Engineering Department. He is the primary author of more than 30 conference and journal papers. From 2011 and up to date, he has been a lecturer in systems modelling and simulation, numerical methods, and automatic control systems modules. He is now an associate professor at the University of Tripoli and is a supervisor of numerous projects in the field of automatic control systems. His research interests concentrate on optimisation, numerical techniques, artificial intelligence control and systems modelling and simulation. Dr Elarbi has been a member of the engineering union since 2001. He has also been a member of the Mathworks community since 2006 and the CFD online society since 2007. He has been a member of AIAA and RAeS since 2008.
Email: ezzely5@yahoo.com

Dina S. Laila was born in Jakarta Indonesia. She received her PhD in Control Engineering from the University of Melbourne in 2003. She joined the Control and Power Group (EE CAP), Electrical and Electronic Engineering Dept., Imperial College London (2003-2006), working mainly in the non-linear control research area. Between 2006 and 2007, she was with the Institute for Design and Control of Mechatronic Systems, Johannes Kepler University Linz, Austria. She returned to Imperial College in 2007 and expanded her research to non-linear control for uncrewed aerial vehicles and the measurement and control for power systems and power system signal analysis. Before joining Southampton, Dina was with the Faculty of Engineering, Kingston University, London (2009-2011). Dina Shona Laila is a Senior Member of the IEEE. She actively serves as a member of the IEEE CSS Conference Editorial Board and as a reviewer in the Control Engineering field.
Email: dina.laila@coventry.ac.uk

Nadjim M. Horri is currently a senior lecturer in aerospace engineering at Coventry University since 2012. He was awarded a PhD in the control of spacecraft from Surrey Space Centre, University of Surrey, 2004. He worked for five years as a research fellow on spacecraft control-related projects. He taught guidance, navigation, and control, as well as the dynamics and control of spacecraft. He teaches UAV systems, aerospace control, flight dynamics, avionics, instrumentation, and aerospace technology. He is currently the course director of the MSc in aerospace engineering at Coventry University. He also teaches Coventry MSc courses to external partners such as Emirates Aviation University.
Email: ab3853@coventry.ac.uk

Appendix I

S. No.	Abbreviation	Description
1	A/C	Aircraft
2	AMPC	Adaptive Model Predictive Control
3	B747	Boeing® 747
4	B747-100/B747-200/B747-400	Boing 747-100/Boing 747-200/Boing 747-400
5	CG	Centre of gravity
6	CSL	Cubic Splines
7	EP	Equilibrium Point
8	FI-LQR	Fractional-Order-Integral-Linear Quadratic Regulator
9	FSF	Full State Feedback
10	FSFLQR	Full State Feedback Linear Quadratic Regulator
11	GS	Gain Scheduling
12	GS-FSFLQR	Gain Scheduling-Full State Feedback Linear Quadratic Regulator
13	GS-LQR	Gain Scheduling-Linear Quadratic Regulator
14	GS-PID	Gain Scheduling-Proportional Integral Derivative
15	IAE	Integral Absolute Error
16	IGWO	Improved Grey Wolf Optimizer
17	IGWO-PD2LQR	Improved Grey Wolf Optimizer-Proportional-Derivative-Derivative-Linear Quadratic Regulator
18	ISE	Integral Square Error
19	ITAE	Integral Time Absolute Error
20	ITSE	Integral Time Square Error
21	JAR	Joint Aviation Requirements
22	LHC	Latin Hypercube
23	LMI	Linear Matrix Inequalities
24	LPV	Linear Parametrically Varying
25	LQR	Linear Quadratic Regulator
26	LQR-LMI	Linear Quadratic Regulator-Linear Matrix Inequalities
27	LTI	Linear Time-Invariant
28	M	Mach number
29	MAC	Mean Aerodynamic Chord
30	PD	Proportional-Derivative
31	PD-LQR	Proportional-Derivative-Linear Quadratic Regulator
32	PD2-LQR	Proportional-Derivative-Derivative-Linear Quadratic Regulator
33	PID	Proportional-Integral-Derivative
34	PID-LQR	Proportional-Integral-Derivative-Linear Quadratic Regulator
35	P-LQR	Proportional-Linear Quadratic Regulator
36	RIAE	Refined Integral Absolute Error
37	RLQR	Robust Linear Quadratic Regulator